Particle & Particle Systems Characterization

www.particle-journal.com

Facile Functionalization of Gold Nanoparticles with PLGA Polymer Brushes and Efficient Encapsulation into PLGA Nanoparticles: Toward Spatially Precise Bioimaging of Polymeric Nanoparticles

Alaaldin M. Alkilany, Samer R. Abulateefeh, and Catherine J. Murphy*

Nanocarriers prepared from poly(lactide-*co*-glycolide) (PLGA) have broad biomedical applications. Understanding their cellular uptake and distribution requires appropriate visualization in complex biological compartments with high spatial resolution, which cannot be offered by traditional imaging techniques based on fluorescent or radioactive probes. Herein, the encapsulation of gold nanoparticles (GNPs) into PLGA nanoparticles is proposed, which should allow precise spatial visualization in cells using electron microscopy. Available protocols for encapsulating GNPs into polymeric matrices are limited and associated with colloidal instability and low encapsulation efficiency. In this report, the following are described: 1) a facile protocol to functionalize GNPs with PLGA polymer followed by 2) encapsulation of the prepared PLGA-capped GNPs into PLGA nanocarriers with 100% encapsulation efficiency. The remarkable encapsulation of PLGA-GNPs into PLGA matrix obeys the general rule in chemistry "like dissolves like" as evident from poor encapsulation of GNPs capped with other polymers. Moreover, it is shown that how the encapsulated gold nanoparticles serve as nanoprobes to visualize PLGA polymeric hosts inside cancer cells at the spatial resolution of the electron microscope. The described methods should be applicable to a wide range of inorganic nanoprobes and provide a new method of labeling pharmaceutical polymeric nanocarriers to understand their biological fate at high spatial resolution.

Polymeric nanocarriers have various biomedical applications including drug delivery, cancer treatment, and biomedical imaging.[1,2] Among many, PLGA is an FDA approved pharmaceutical polymer with broad biomedical applications and a proven presence in the clinic/market.[3] Interaction of PLGA nanocarriers with cells is usually studied using fluorescent or radioactive labeling, which both suffer from poor spatial resolution. In addition, molecular leaching and photobleaching are serious limitations to conventional fluorescent labeling,[4–6] whereas the use of radioactive labeling requires special handling and analysis. Alternatively, inorganic nanocrystals with fascinating optical, electronic, and magnetic properties have been used to label PLGA and other polymeric nanoparticles and thus allow for novel tracking and visualization experiments. Examples of such nanoparticles include gold nanoparticles (GNPs), magnetic iron oxide nanoparticles, and fluorescent quantum dots; these materials have been utilized for computed tomography (CT) based imaging, MRI imaging and fluorescent based imaging, respectively, at the organ level.[7–12] However, visualizing PLGA (and other polymeric) nanoparticles inside cells or biological compartments at extremely high spatial resolution requires electron microscopy (EM)-based imaging, allowing deeper understanding of their fate at the subcellular level. Polymeric nanocarriers are electron transparent and cannot be visualized in cells or tissues using electron microscopy (EM) without careful and tedious staining that frequently shows serious artifacts. In contrast, GNPs are electron dense and thus can be visualized by EM and quantified, albeit destructively, with inductively coupled plasma mass spectrometry (ICP-MS).[13,14] These physiochemical properties of GNPs combined with its biocompatibility and ease of synthesis make them ideal "nanoprobes" to understand the nano-biointerface.[13,14]

PLGA is a hydrophobic polymer that dissolves in organic solvents.[3] PLGA nanoparticles are typically prepared using two methods: 1) the nanoprecipitation method, in which PLGA is dissolved in a water-miscible organic solvent such as acetone and then precipitated into nanoparticles upon addition into a nonsolvent (e.g., water); 2) the emulsion-evaporation method, in which PLGA is dissolved in a water-immiscible organic solvent such as dichloromethane, which is emulsified into an aqueous

Dr. A. M. Alkilany, Dr. S. R. Abulateefeh
Department of Pharmaceutics & Pharmaceutical Technology
School of Pharmacy
The University of Jordan
Amman 11942, Jordan
E-mail: a.alkilany@ju.edu.jo
Prof. C. J. Murphy
Department of Chemistry
University of Illinois at Urbana-Champaign
600 South Mathews Avenue, Urbana, IL 61801, USA
The ORCID identification number(s) for the author(s) of this article can be found under https://doi.org/10.1002/ppsc.201800414.

DOI: 10.1002/ppsc.201800414

external phase followed by evaporation of the organic solvent to form PLGA nanoparticles.[6] Obviously, efficient encapsulation requires dissolving both PLGA polymer and drug into the organic solvent (acetone or dichloromethane), and thus PLGA nanoparticles typically encapsulate hydrophobic rather than hydrophilic drugs. With this in mind, and to encapsulate GNPs into PLGA nanoparticles, the former should be hydrophobic and exhibit an excellent colloidal stability in organic solvents. Although hydrophobic alkane-capped inorganic nanocrystals (3–5 nm in diameter) would partially fulfill such criteria, they failed to exhibit sufficient colloidal stability in a number of organic solvents such as acetone. More importantly, the organic routes used to prepare these hydrophobic nanocrystals have less potential to tune/control nanoparticle size and shape in comparison to the aqueous routes.[13,14] On the other hand, inorganic nanocrystals prepared by the aqueous routes require post-synthesis surface hydrophobication which is a clear challenge in the case of large nanoparticles, calling for a simple and reliable protocol as the one presented herein by our group.

In this communication, we describe 1) a facile, simple, and highly reproducible hydrophobication of citrate-capped GNPs (Cit-GNPs) with thiolated polymers (namely polyethylene glycol (PEG-SH), polystyrene (PS-SH), and poly(lactic-*co*-glycolic acid) (PLGA-SH), which all impart GNPs with excellent colloidal stability in both acetone and dichloromethane; and 2) efficient encapsulation of PLGA-capped GNPs, but, interestingly, not PEG-GNPs or PS-GNPs into PLGA nanocarriers, which highlight the importance of miscibility between polymer that decorates the surface of GNPs and the host nanocarrier's matrix; 3) visualization of PLGA nanoparticles inside the cellular cytoplasm at the spatial resolution of the electron microscopy using encapsulated GNPs as probes.

Cit-GNPs (15 nm in diameter) were prepared using a modified aqueous Frens method.[15] These nanoparticles are capped with weakly physisorbed citrate anions with proven biocompatibility and ease of displacement with other ligands. Previously, we reported a facile phase transfer of GNPs from water to dichloromethane using PEG-SH as the phase transfer and capping agent.[16] Remarkably, the same protocol resulted in a facile transfer of GNPs from water to dichloromethane using PS-SH or PLGA-SH (**Figure 1**). Addition of methanol as a common solvent to a biphasic system of an aqueous Cit-GNPs suspension and dichloromethane containing either PEG-SH, PS-SH, or PLGA-SH results in immediate and complete phase transfer of GNPs from the aqueous layer to the dichloromethane as evident from the complete transfer of the red color to the lower organic layers in Figure 1. A red shift in the localized surface plasmon resonance of the polymer capped-GNPs in dichloromethane (8 nm, due to higher refractive index of the organic solvent) without peak broadening is indicative of successful phase transfer without nanoparticle aggregation (Figure 1C).[17] No phase transfer was observed when nonthiolated polymers were used or in the absence of any polymer (control experiments) (Figure 1B), confirming the role of the thiol-gold strong bond to drive the assembly of polymer brushes on GNPs and to displace the weakly physisorbed citrate anions.[16,18] The phase transfer was scalable for larger batches as shown in Figure 1D and the final particles showed a remarkable colloidal stability in dichloromethane. We note that the transferred GNPs can be dried completely from dichloromethane and suspended with excellent colloidal stability in other organic solvents that dissolve the polymer. For example, transferred GNPs with PLGA-SH can be dried and suspended in "common solvents for PLGA" including acetonitrile, acetone, dimethyl sulfoxide (DMSO), dichloromethane, chloroform, THF, and toluene but not in "PLGA nonsolvents" such as water, methanol, and hexane (Figure S1, Supporting Information), which further confirms the successful hydrophobication and capping of GNPs with PLGA polymer. While phase transfer using small ligands such as alkanethiols is size dependent and fails at large nanoparticles, our phase transfer protocol can be applied for Cit-GNPs with various sizes (10 and 65 nm in diameter) as shown in Figure S2 (Supporting Information). We note that the facile transfer of GNPs from water to the organic phase using PEG-SH, PS-SH, or PLGA-SH suggest the broad applicability of our phase transfer protocol and could be employed to functionalize GNPs with other thiolated hydrophobic polymers.

Our initial design to encapsulate GNPs into PLGA nanocarriers suggested the use of PEG-GNPs due to the biocompatibility of PEG molecules and the excellent colloidal stability of PEG-GNPs in the organic solvents used to prepare PLGA nanoparticles (acetone and dichloromethane). However, encapsulation of PEG-GNPs into PLGA nanoparticles using the nanoprecipitation method was not successful as evident from the empty PLGA nanoparticles in TEM images (**Figure 2**B). Using the emulsion-evaporation method resulted in a similar poor encapsulation (marginally better compared to the nanoprecipitation method with few GNPs inside PLGA nanoparticles as shown in **Figure 3**). The poor encapsulation of PEG-GNPs into PLGA can be explained by the dual hydrophilic–hydrophobic character of the PEG molecule (high solubility in both water and organic solvents), which results in partitioning of PEG-GNPs into the external aqueous phase, leaving the PLGA nanoparticles empty, similar to the well documented poor encapsulation of hydrophilic drugs into PLGA nanoparticles (partitioning of PEG-GNPs into the water phase is sketched in Figure 2A).[3,19] To minimize this partitioning, we then examined the encapsulation of more hydrophobic GNPs, namely, polystyrene-capped GNPs (PS-GNPs). PS-GNPs showed excellent colloidal stability in acetone and dichloromethane but failed to result in efficient encapsulation into PLGA nanoparticles using the nanoprecipitation or the emulsion-evaporation method, as evident from TEM images in Figures 2B and 3, respectively. Severe black aggregates were observed during encapsulation of PS-GNPs using the nanoprecipitation method resulting mostly in empty PLGA nanoparticles (Figure 2B). Using the emulsion-evaporation method to encapsulate PS-GNPs resulted mostly in empty PLGA nanoparticles with very few PLGA nanoparticles loaded with large quantity of aggregated GNPs as shown in Figure 3. Despite its extreme hydrophobicity, the poor encapsulation of PS-GNPs can be explained by the poor miscibility of PS with PLGA. Both polymers (PS and PLGA) are hydrophobic but they have different solubility profiles and thus form immiscible polymer blends (phase separation is sketched in Figure 2A). For example, PLGA is not soluble in cyclohexane where PS can be selectively dissolved from PLGA/PS blend by the same solvent.[20] Phase separation in PS and poly(lactide) (similar polymer to PLGA) blend were reported recently in the shell of polymeric microcapsule with

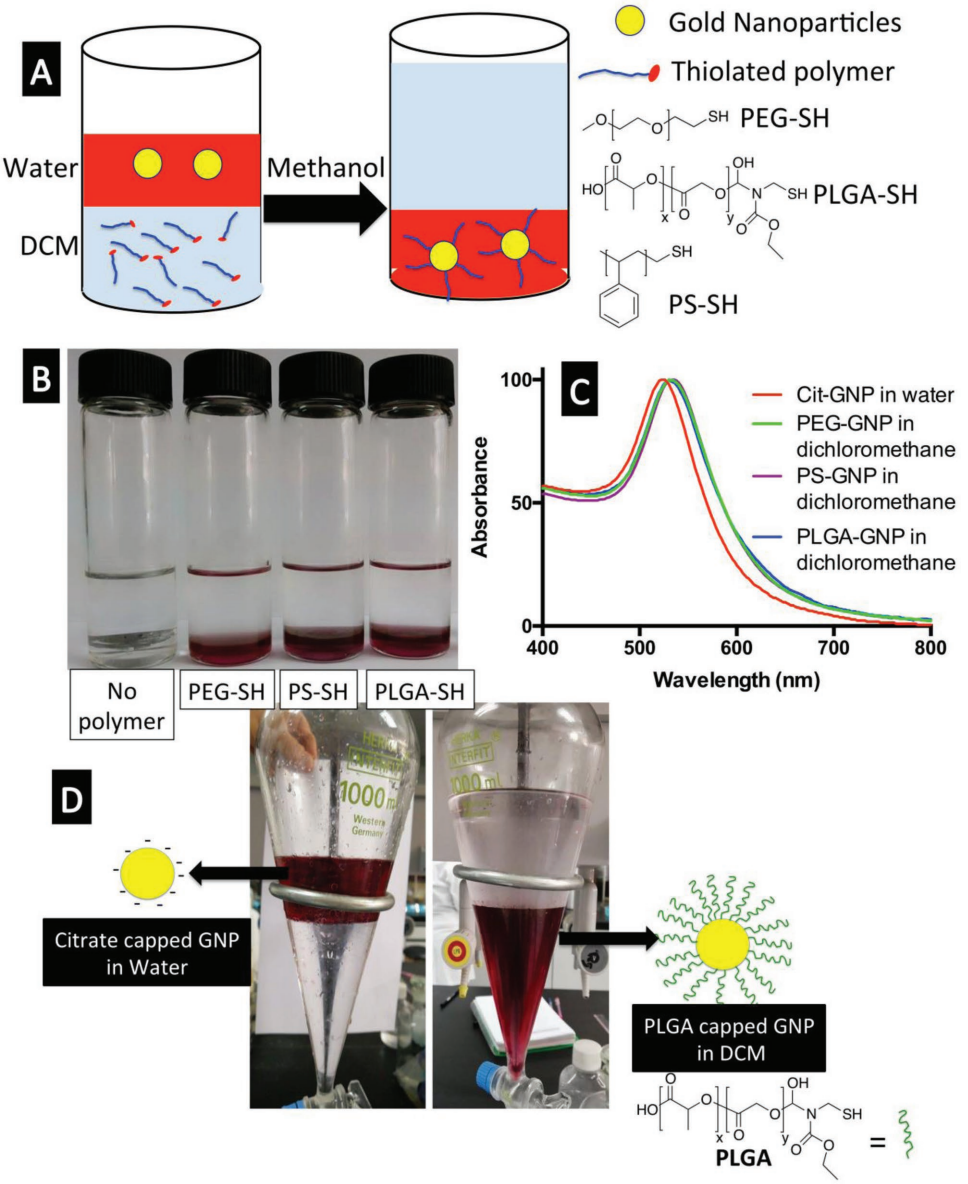

Figure 1. A) Sketch demonstrates the phase transfer of citrate-capped gold nanoparticles from water to dichloromethane (DCM) containing thiolated polymers (PEG-SH, PLGA-SH, and PS-SH, chemical structures are shown to the right). B) Vial images of polymer-capped gold nanoparticles in dichloromethane (red lower layer in each vial) after phase transfer using PEG-SH, PLGA-SH, or PS-SH as labeled (upper layer in each vial is the aqueous phase). C) UV–vis spectra of PEG-GNPs, PLGA-GNPs, or PS-GNPs in dichloromethane after phase transfer compared to citrate-capped GNPs in water. D) Large scale phase transfer of citrate-capped GNPs from water to dichloromethane containing PLGA-SH.

selective solubilization of the former to create porous shells.[21] In fact, and according to the Flory–Huggins theory, most polymers should be immiscible as ΔG_{mix} is always positive with only few examples on miscible polymer blends.[22,23]

Our failures to encapsulate PEG-GNPs and PS-GNPs into PLGA matrix motivated us to evaluate the encapsulation process using PLGA-capped GNPs (PLGA-GNPs) taking into consideration the general rule in chemistry "like dissolves like." Our hypothesis is that capping GNPs with PLGA brushes should ensure: 1) excellent colloidal stability of PLGA-GNPs in "solvents of PLGA;" 2) Insolubility of PLGA-GNPs in "antisolvents of PLGA" and thus minimizing the partitioning and loss into the external aqueous phase during encapsulation; and 3) high intrinsic miscibility/affinity of PLGA-GNPs to the PLGA matrix to ensure efficient encapsulation as can be predicted relying on the "like dissolves like" principle.

In agreement with our hypothesis, dissolving both PLGA-GNPs and PLGA polymer in acetone or dichloromethane allows a facile encapsulation of GNPs into the PLGA nanoparticles through conventional nanoprecipitation (Figure 2B) or emulsion-evaporation method (Figure 3). Transmission electron microscope images in the two figures show excellent encapsulation of GNPs into PLGA nanocarriers with no free GNPs in the background. Highly efficient encapsulation

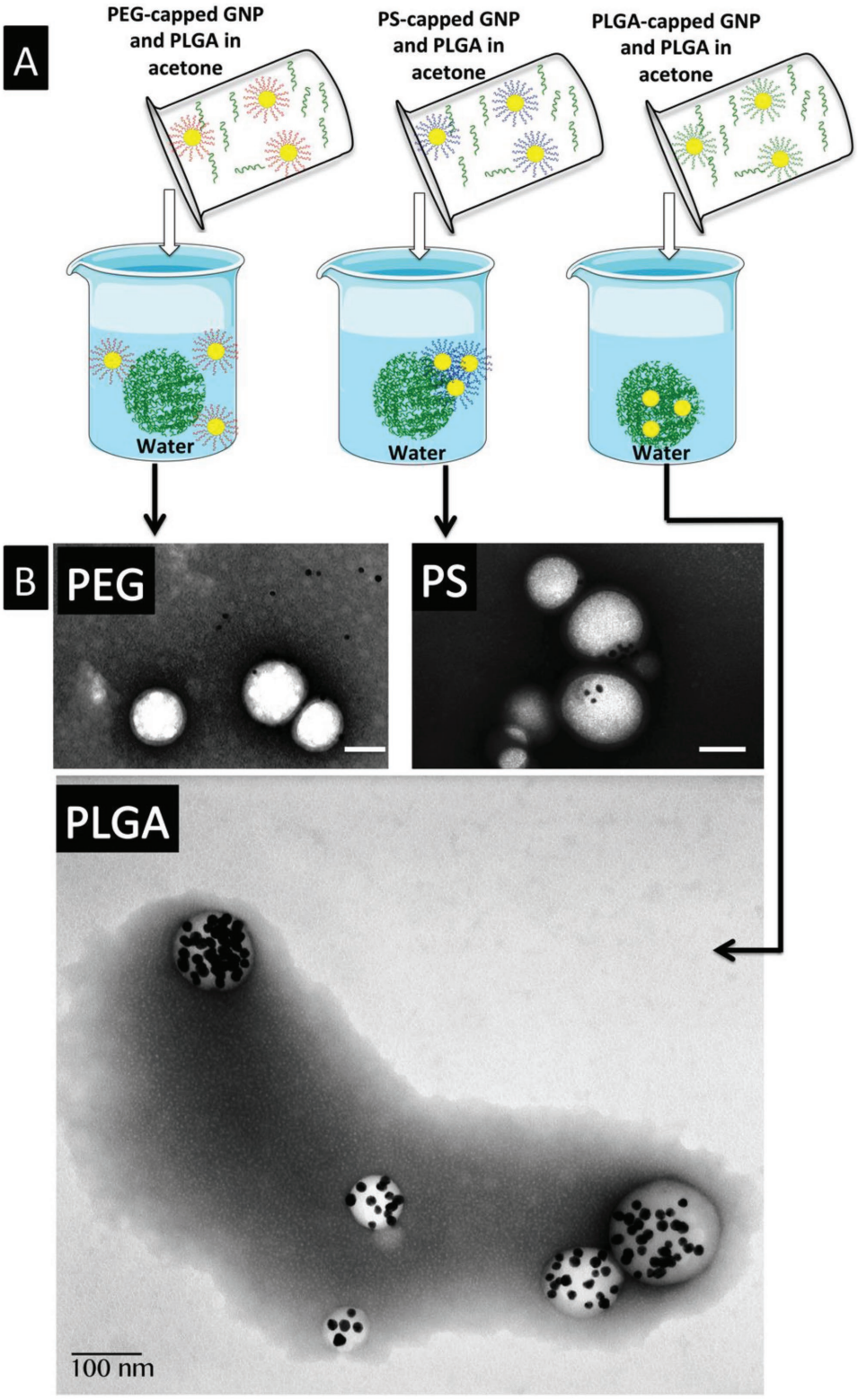

Figure 2. A) Cartoon illustrates our hypothesis of efficient encapsulation of GNPs into PLGA nanoparticles according to the "like dissolves like" principle. This cartoon demonstrates the nanoprecipitation method using PEG-GNPs (left), PS-GNPs (middle), and PLGA-GNPs (right). PEG-GNPs partition in to the water phase due to the hydrophilicity of PEG molecules. The hydrophobicity of PS-GNPs does not guarantee efficient encapsulation but instead results in phase separation due to immiscibility into the PLGA matrix. The use of PLGA-GNPs resulted in efficient encapsulation in agreement to the "like dissolves like" principle. B) TEM images with negative staining of PLGA nanoparticles encapsulated with PEG-GNPs, PS-GNPs, or PLGA-GNPs, prepared using the nanoprecipitation method. Scale bars are 100 nm in all images.

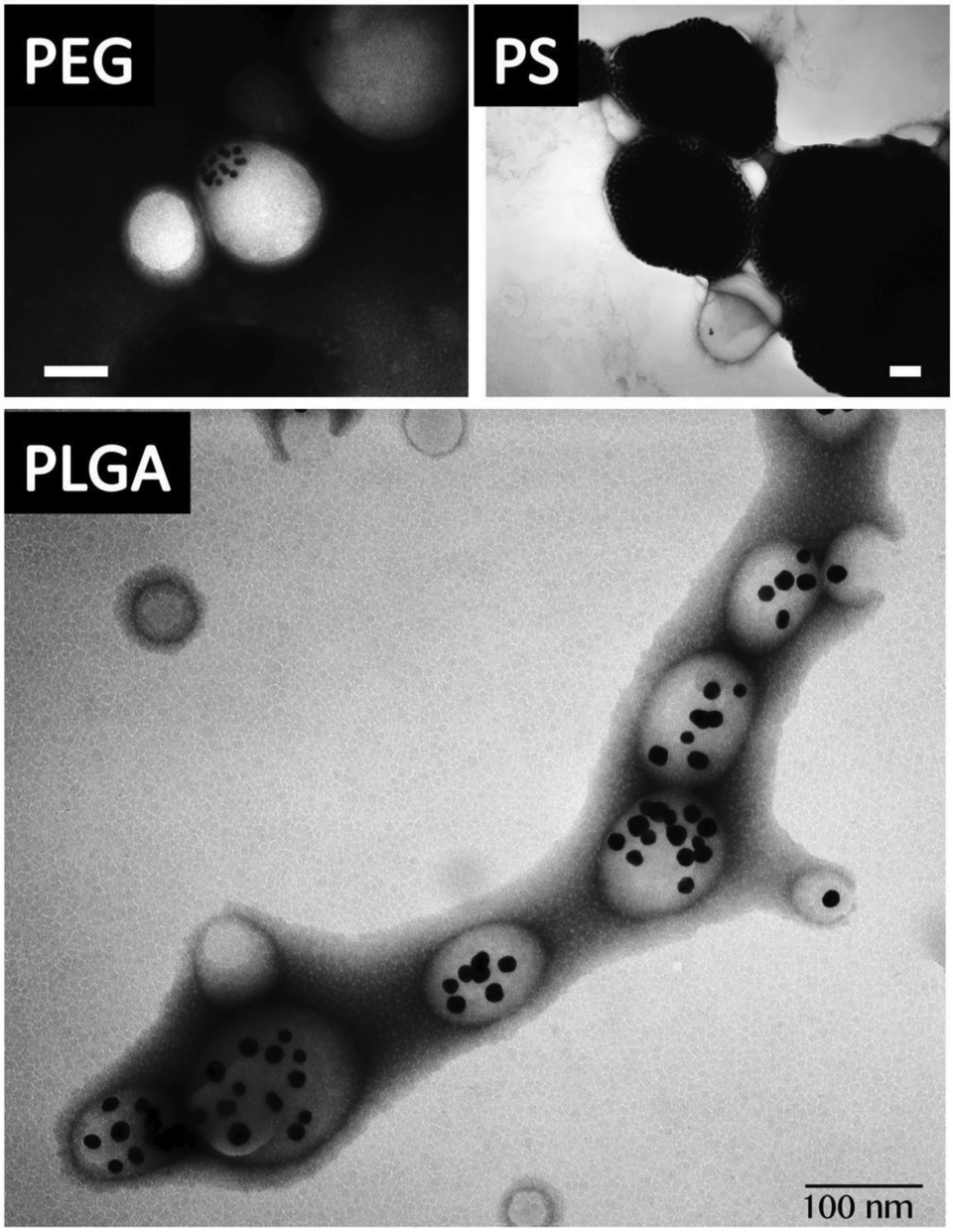

Figure 3. TEM images with negative staining of PLGA nanoparticles encapsulated with PEG-GNPs, PS-GNPs, or PLGA-GNPs, prepared using the emulsion–evaporation method. Scale bars are 100 nm in all images.

(100% efficiency) was confirmed by ICP-MS analysis (method is detailed in Figure S3 of the Supporting Information). Moreover, the encapsulated amount of PLGA-GNPs into PLGA nanocarriers can be tuned by controlling the initial ratio between PLGA-GNPs and PLGA polymer during the encapsulation procedure (Figure S4, Supporting Information). To confirm that GNPs are located inside the PLGA nanoparticles, TEM images were collected at various focal planes where GNPs can be seen, indicating encapsulation into the matrix rather than adsorbing on the surface of PLAG nanoparticles (data not shown). Moreover, encapsulated GNPs into PLGA nanocarriers exhibited unusual chemical stability against etching with strong oxidizing agents such as potassium cyanide, suggesting that GNPs are embedded in hydrophobic matrix that cyanide ions cannot penetrate, which further confirms the presence of GNPs inside the PLGA nanoparticles (Figure S5, Supporting Information). In contrast, cyanide ions etch GNPs when mixed with PLGA nanoparticles (physical mixture serves as a control here) as shown in Figure S5 (Supporting Information). The observed resistance of encapsulated GNPs into hydrophobic PLGA nanocarriers to cyanide etching resembles the reported resistance of GNPs to cyanide when they are coated with lipid bilayers.[24] Collectively, it can be concluded that when the capping agent of inorganic nanoparticles is identical to the matrix-forming polymer, excellent "chemical compatibility/miscibility" is guaranteed resulting in a facile encapsulation, as

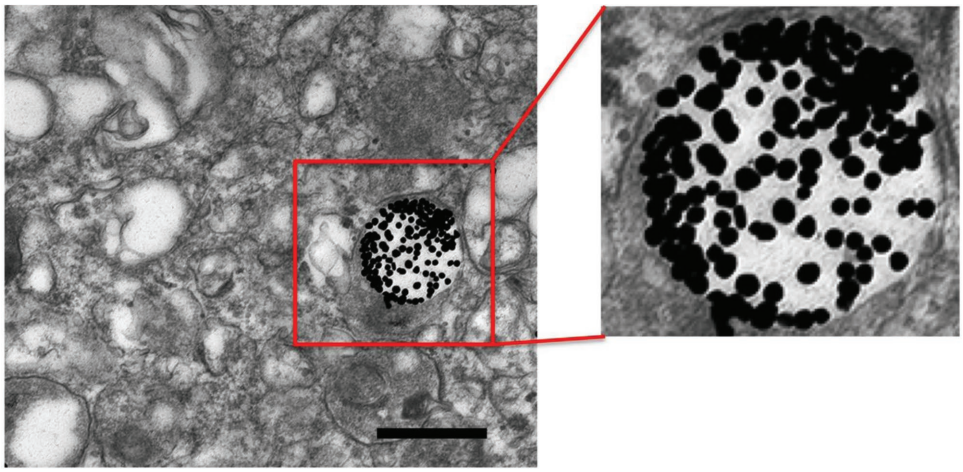

Figure 4. Visualization of PLGA nanoparticle cellular uptake using GNPs as probes. TEM image of a single PLGA nanoparticle encapsulating GNPs inside the cytoplasm of HeLa cells (insert is a closer view). Scale bar is 150 nm.

in the case of PLGA-GNPs into PLGA nanocarriers. This notion is important for optimal surface engineering of inorganic nanoprobes for efficient encapsulation into polymeric nanocarriers or matrices. In addition to the high efficiency, the simplicity of our protocol is a clear advantage over available limited protocols to label PLGA nanocarriers with GNPs. For example, Mieszawska et al. reported the labeling of PLGA nanoparticles with GNPs for CT imaging using a complex encapsulation procedure that relies on repetitive esterification reactions (rounds of covalent conjugation of PLGA to nanocrystals using EDC chemistry).[7] Clearly, our functionalization of GNPs with PLGA and encapsulation into PLGA nanoparticles is much simpler and does not require lengthy and complex chemistry.

It is important to mention that the exact number of GNPs in each PLGA nanoparticles (as quantitative probability distribution) requires single particle separation/analysis and cannot be obtained directly from 2D TEM images that capture only a random focal plane depending on the size of PLGA nanoparticles. Alternatively, we determined the average number of GNPs encapsulated into one PLGA nanocarrier by counting the total number of PLGA nanocarriers using tunable resistive pulse sensing (qNANO, Izon Science) coupled to ICP-MS analysis to measure the number of GNPs in the same sample (Figure S6, Supporting Information). Our analysis revealed an average of 33 GNPs per PLGA nanocarrier from similar preparations to Figure 2. However, we believe that the particle size of GNPs and loading extent of GNPs into PLGA are critical attributes to control the homogenous distribution of GNPs in PLGA nanoparticles, which is the subject of on-going research. To test the ability to visualize PLGA nanocarriers with encapsulated GNPs in a biological compartment, we dosed HeLa cancer cells with PLGA nanoparticles encapsulated with GNPs for 24 h and then we visualized the collected cells using TEM (we would like to mention that understanding the intracellular biodistribution of PLGA nanoparticles or the extent/mechanism of their cellular uptake is not the scope of this communication and is the subject of on-going research). Due to the presence of GNPs probes, PLGA nanocarriers can be clearly seen inside cell with high spatial resolution (**Figure 4**), which cannot be obtained by alternative conventional visualization techniques such as fluorescent microscopy.

In conclusion, we developed a facile phase transfer protocol to functionalize GNPs with PLGA brushes, which resulted in efficient encapsulation into PLGA nanocarriers. Moreover, the poor encapsulation of PEG-GNPs and PS-GNPs highlights the importance of nanoparticle's surface chemistry as a critical parameter determines encapsulation efficiency. When GNPs have same polymer brushes for the host matrix, the "like dissolves like" rule operates and efficient encapsulation is observed. The encapsulation of GNPs as electron dense nanoprobes allowed spatially precise allocation of electron transparent polymeric nanocarriers. We believe that this work will pave the road for precise evaluation of the intracellular distribution of pharmaceutical polymeric nanotherapeutics, which ultimately should enrich our understanding of their nano-biointeractions.

Experimental Section

Synthesis of Citrate-Capped Gold Nanoparticles: Cit-GNPs were synthesized using the Frens method with modification.[15] An aqueous solution of $HAuCl_4$ (100 mL, 0.25×10^{-3} M) was heated in a conical flask and brought to boil. To the boiling solution, 3.0 mL of an aqueous solution of 1% (w/w) sodium citrate was added. The heating was maintained until a deep ruby red color appeared (about 10 min), indicating the formation of GNPs. Transmission electron microscopy, zeta potential analyzer, and UV–vis spectrophotometry measurements were used to evaluate the prepared nanoparticles.

Phase Transfer of Cit-GNPs to Dichloromethane with Thiolated Polymers: As prepared Cit-GNPs in aqueous media (5×10^{-9} M in particles, 20 mL) was added to dichloromethane containing the thiolated polymers (1 mg mL^{-1} of either PEG-SH, PLGA-SH, or PS-SH, 20 mL). Vigorous hand shaking followed immediately by adding 30 mL methanol resulted in the transfer of all GNPs from the aqueous layer to the organic layer.

Encapsulation of Polymer-Capped GNPs into PLGA Nanoparticles Using the Nanoprecipitation Method: Polymer-capped GNPs (either PEG-SH, PLGA-SH, or PS-SH) were dried from dichloromethane after phase transfer and suspended in acetone (2 mL of 2×10^{-9} M GNPs)

into which, PLGA (20 mg) was dissolved. Polymer-capped GNPs/PLGA in acetone was then added drop wise to deionized water with stirring. The nanoparticle suspension was left stirring to allow evaporation of acetone.

Encapsulation of Polymer-Capped GNPs into PLGA Nanoparticles Using the Emulsion-Evaporation method: PLGA (50 mg) was dissolved in dichloromethane containing polymer-capped GNPs (either PEG-SH, PLGA-SH or PS-SH) (5 mL, 2×10^{-9} M) and then emulsified into Pluronic F127 aqueous solution (10 mL, 7% w/v) using tip sonicator (Sonics VC 750, 3 mm tapered microtip screws into 13 mm threaded end probe, Sonics & Materials, Inc) for 3 min (40% power) on ice bath. Emulsion was stirred overnight to allow evaporation of dichloromethane and the formation of PLGA nanoparticles. Hydrodynamic diameter and polydispersity index (PDI) of prepared PLGA nanoparticles were measured by dynamic light scattering using Zetasizer Nano-ZS (Malvern instruments, UK).

TEM Imaging of GNPs Encapsulated in PLGA Nanoparticles: Nanoparticle suspension was centrifuged and a drop from the pellet was placed on clean parafilm sheet. A copper grid, coated with formvar was placed on top of the sample droplet for 10 min. The excess sample was then removed with filter paper and the grid placed on 2% ammonium molybdate or uranyl acetate for 2 min. The grid was then dried by removing the excess fluid with filter paper, placed into a grid box, and covered with drierite crystal for 10 min. The grid was then examined in the Hitachi H600 Transmission Electron Microscope at 75 KV.

ICP-MS Analysis: The concentration of gold in samples was measured with ICP-MS. For the sample preparation, 150 µL of freshly prepared aqua regia ($HCl:HNO_3 = 3:1$) was added to 50 µL of the sample, and the mixture was kept in an autoshaker for overnight at room temperature. Afterward, 1.8 mL of Milli-Q water was added (final solution volume = 2 mL and the dilution factor is 40). Before the measurement took place, the ICP-MS setup was calibrated with a freshly prepared serial dilution of Au (Roth Standard (1000 mg mL^{-1})). The calibration curve was constructed using a concentrations series from 2 to 2500 parts per billion (ppb). Additionally, the auto tuning solution from Agilent for ICP-MS 7500 cs with a standard concentration of 1 µg L^{-1} of Ce, Co, Li, Mg, Tl, and Y was used to set the general background as well as to calibrate the electrical field of the lenses and the magnetic quadrupole field in strength and frequency. In the calibrated setup, the oxidation species rate was lower than 0.8% and double charge rate was below 2%. The samples were introduced into the ICP MS setup through a perfluoroalkoxy alkane (PFA) based microflow spray chamber, where the aqueous sample was nebulized, introduced into the argon gas flow, and transported to the torch, where it was ionized in an argon plasma of around 6000 °C. After ionization, the sample was presorted using an omega lens, element wise separated in a quadrupole field through the mass to charge rate, again sorted using kinetic barriers and a charged lens system, and finally detected with either an analog or a digital detector depending on the count rate and interpreted using the calibration curve which usually transfer the CPS values into elemental concentrations. The raw data were then multiplied by the dilution factor to get the actual concentrations of the samples.

TEM Imaging of GNPs in Cultured Cells: Hela cells were plated at 50 000 cells mL^{-1} in 6-well plates and incubated for 48 h until confluency was reached. The cells were then dosed with PLGA nanoparticles encapsulating GNPs for 24 h. Cells were then washed, trypsinized, and dispersed in Karnovsky's fixative. Cells were then centrifuged; the pellet was embedded using osmium tetroxide, potassium ferrocyanide, uranyl acetate, dehydrated with ethanol and acetonitrile, and embedded in an Epon mixture (Lx112 – Ladd, Inc.), polymerized, and sectioned at 60–100 nm using a diamond knife and a Reichart ultra-microtome. Sections were placed on copper grids and stained with uranyl acetate and lead citrate. Cellular imaging was performed on a Hitachi H600 microscope operating at 75 kV.

Counting of PLGA Nanoparticles: The concentration and diameter of PLGA nanoparticles was determined by TRPS (Tunable Resistive Pulse Sensing) technology using a qNANO Gold device (Izon Science). A pore membrane (NP150) was placed on a fluid cell of qNano then ion current was confirmed by 1/3 PBS solution. After the conduction of the device, PBS solution on the fluid cell was replaced with PLGA suspension. The applied pressure, stretch, and voltage were 10 kPa, 47.01 mm, and 1.5 V, respectively. For the calculation of particle size, genuine standard nanoparticle solution (CPC100B, mode size: 110 nm, mean size: 110 nm, raw concentration: 1.1×10^{13} particles mL^{-1}) was used.

Supporting Information

Supporting Information is available from the Wiley Online Library or from the author.

Acknowledgements

A.M.A. acknowledges funding from the Deanship for Scientific Research at the University of Jordan and the Scientific Research Support Fund (SRSF) grant number MPH/1/6/2014 for financial support. The authors acknowledge the assistance of Izone Science Ltd in particle counting experiments and Dr. Lou Ann Miller of the Materials Research Laboratory at UIUC for the bio-TEM images.

Conflict of Interest

The authors declare no conflict of interest.

Keywords

encapsulation, gold nanoparticles, phase transfer, PLGA

Received: October 2, 2018
Revised: November 8, 2018
Published online: December 14, 2018

[1] D. Rosenblum, N. Joshi, W. Tao, J. M. Karp, D. Peer, *Nat. Commun.* **2018**, *9*, 1410.
[2] B. L. Banik, P. Fattahi, J. L. Brown, *Wiley Interdiscip. Rev.: Nanomed. Nanobiotechnol.* **2016**, *8*, 271.
[3] F. Danhier, E. Ansorena, J. M. Silva, R. Coco, A. Le Breton, V. Préat, *J. Controlled Release* **2012**, *161*, 505.
[4] G. Bastiat, C. O. Pritz, C. Roider, F. Fouchet, E. Lignières, A. Jesacher, R. Glueckert, M. Ritsch-Marte, A. Schrott-Fischer, P. Saulnier, J.-P. Benoit, *J. Controlled Release* **2013**, *170*, 334.
[5] C. Simonsson, G. Bastiat, M. Pitorre, A. S. Klymchenko, J. Béjaud, Y. Mély, J.-P. Benoit, *Eur. J. Pharm. Biopharm.* **2016**, *98*, 47.
[6] M. M. A. Abdel-Mottaleb, A. Beduneau, Y. Pellequer, A. Lamprecht, *Int. J. Pharm.* **2015**, *494*, 471.
[7] A. J. Mieszawska, A. Gianella, D. P. Cormode, Y. Zhao, A. Meijerink, R. Langer, O. C. Farokhzad, Z. A. Fayad, W. J. Mulder, *Chem. Commun.* **2012**, *48*, 5835.
[8] Y. Qiu, R. Palankar, M. Echeverría, N. Medvedev, S. E. Moya, M. Delcea, *Nanoscale* **2013**, *5*, 12624.
[9] Y. Jia, M. Yuan, H. Yuan, X. Huang, X. Sui, X. Cui, F. Tang, J. Peng, J. Chen, S. Lu, W. Xu, L. Zhang, Q. Guo, *Nanomedicine* **2012**, *7*, 1697.
[10] J. Kim, J. E. Lee, S. H. Lee, J. H. Yu, J. H. Lee, T. G. Park, T. Hyeon, *Adv. Mater.* **2008**, *20*, 478.
[11] A. Topete, D. Melgar, M. Alatorre-Meda, P. Iglesias, B. Argibay, S. Vidawati, S. Barbosa, J. A. Costoya, P. Taboada, V. Mosquera, *J. Mater. Chem. B* **2014**, *2*, 6967.

[12] A. Topete, M. Alatorre-Meda, E. M. Villar-Alvarez, S. Carregal-Romero, S. Barbosa, W. J. Parak, P. Taboada, V. Mosquera, *Adv. Healthcare Mater.* **2014**, *3*, 1309.
[13] A. M. Alkilany, S. E. Lohse, C. J. Murphy, *Acc. Chem. Res.* **2013**, *46*, 650.
[14] E. C. Dreaden, A. M. Alkilany, X. Huang, C. J. Murphy, M. A. El-Sayed, *Chem. Soc. Rev.* **2012**, *41*, 2740.
[15] G. Frens, *Nat. Phys. Sci.* **1973**, *241*, 20.
[16] A. M. Alkilany, A. I. B. Yaseen, J. Park, J. R. Eller, C. J. Murphy, *RSC Adv.* **2014**, *4*, 52676.
[17] K. L. Kelly, E. Coronado, L. L. Zhao, G. C. Schatz, *J. Phys. Chem. B* **2003**, *107*, 668.
[18] H. Häkkinen, *Nat. Chem.* **2012**, *4*, 443.
[19] J. M. Barichello, M. Morishita, K. Takayama, T. Nagai, *Drug Dev. Ind. Pharm.* **1999**, *25*, 471.
[20] A. Baklavaridis, I. Zuburtikudis, C. Panayiotou, *Polym. Eng. Sci.* **2015**, *55*, 1856.
[21] B. Kim, T. Y. Lee, A. Abbaspourrad, S.-H. Kim, *Chem. Mater.* **2014**, *26*, 7166.
[22] N. Goonoo, A. Bhaw-Luximon, D. Jhurry, *Polym. Int.* **2015**, *64*, 1289.
[23] S. Krause, in *Pure and Applied Chemistry*, Vol. *58*, **1986**, pp. 1553–1560, https://doi.org/10.1351/pac198658121553.
[24] S. Sitaula, M. R. Mackiewicz, S. M. Reed, *Chem. Commun.* **2008**, 3013.

